IBA Logo Here
(missing picture file)

Spora Logo Here
(missing picture file)

ISSN 2473-3067 (Print)
ISSN 2473-5493 (Online)

Examining the Electrical Excitation, Calcium Signaling, and Mechanical Contraction Cycle in a Heart Cell

Kristen Deetz[1], Nygel Foster[2], Darius Leftwich[2], Chad Meyer[3], Shalin Patel[4], Carlos Barajas[5], Matthias K. Gobbert[5,*], Zana Coulibaly[6]

*Correspondence:
Prof. Matthias K. Gobbert, Department of Mathematics and Statistics, University of Maryland, Baltimore County (UMBC), 1000 Hilltop Circle, Baltimore, MD 21250, USA
gobbert@umbc.edu

Abstract

As the leading cause of death in the United States, heart disease has become a principal concern in modern society. Cardiac arrhythmias can be caused by a dysregulation of calcium dynamics in cardiomyocytes. Calcium dysregulation, however, is not yet fully understood and is not easily predicted; this provides motivation for the subsequent research. Excitation-contraction coupling (ECC) is the process through which cardiomyocytes undergo contraction from an action potential. Calcium induced calcium release (CICR) is the mechanism through which electrical excitation is coupled with mechanical contraction through calcium signaling. The study of the interplay between electrical excitation, calcium signaling, and mechanical contraction has the potential to improve our understanding of the regular functioning of the cardiomyocytes and help us understand how any dysregulation can lead to potential cardiac arrhythmias. ECC, of which CICR is an important part, can be modeled using a system of partial differential equations that link the electrical excitation, calcium signaling, and mechanical contraction components of a cardiomyocyte. We extend a previous model [Angeloff, Barajas, et al., Examining the effect of introducing a link from electrical excitation to calcium dynamics in a cardiomyocyte, *Spora: A Journal of Biomathematics*, 2, 2016] to implement a seven variable model that includes for the first time the mechanical component of the ECC. We study how the interaction of electrical and calcium systems can impact the cardiomyocyte's levels of contraction.

Keywords: Heart disease, Heart cell, Cardiac arrhythmia, Excitation-contraction coupling, Calcium Induced Calcium Release

1 Introduction

The leading cause of death in the United States is currently heart disease [9]. However, in order to continue searching for methods to combat heart disease, it is vital that the heart and its underlying processes are understood with greater depth. The importance of having a greater understanding of the heart provides the motivation for this research.

The line of work of this project focuses a single cardiac cell and uses a mathematical model in order to represent the electrical excitation, calcium signaling, and mechanical contraction components of a cardiomyocyte. The original model for calcium induced calcium release (CICR) was introduced in [6, 7] with a three variable model and included only calcium signaling. This original model comprises the heart of the Calcium Signaling component of the system indicated in Figure 1.1. The model was extended for the first time to include the Electrical Excitation component in Figure 1.1 in [1], which implemented a one-way interaction from electrical excitation to calcium signaling indicated by link ① in Figure 1.1. Studies with six variables in [2] extended the coupling to include a two-way cycle between electrical excitation and calcium signaling by incorporating both links ① and ② in Figure 1.1. The 2016 paper [2] also introduced the formulation of the complete eight variable model for all components in Figure 1.1, but not all model variables were used in the simulations, and the studies did not incorporate the mechanical system.

This work studies the introduction of the Mechanical Contraction component in Figure 1.1 by activating the links ③ and ④ in Figure 1.1. This is facilitated by adding a buffer species whose concentration can be related to the contraction of the cell. Thus, this work uses a model with seven variables to represent the excitation-

[1]Department of Mathematics, Eastern University, [2]Department of Computer Science and Electrical Engineering, UMBC, [3]Department of Mathematics, University of Pittsburgh, [4]Department of Computer Science and Mathematical Science, Kean University, [5]Department of Mathematics and Statistics, UMBC, [6]Department of Pharmacology, University of California, Davis

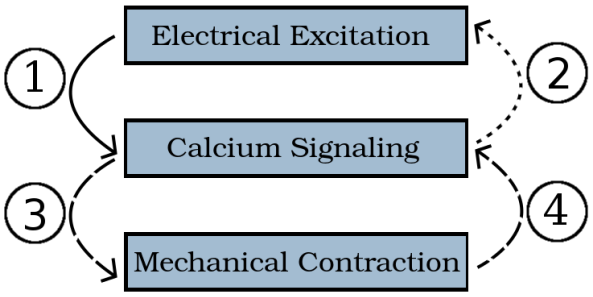

Figure 1.1: The three components of the model and their links labeled ① to ④.

contraction coupling (ECC) occurring in the cardiomyocyte, in which CICR is the mechanism through which electrical excitation is coupled with mechanical contraction through calcium signaling.

The results of the simulations in this paper allow us to draw two key conclusions about the extension of the model and its implementation: The model is capable of connecting the voltage to the contraction of the heart cell via the cytosol calcium and the third buffer species, see the end of Section 5.1; and a stronger coupling strength from voltage to calcium leads to stronger contraction, see the end of Section 5.2. These initial results for the newly extended model make future simulations promising in their predictive capability.

This paper is organized as follows: Section 2 explains the physiological background behind the system being studied. Section 3 specifies the exact model with all equations, formulas, and parameter values of the seven variable model used in this work. Section 4 summarizes the numerical method used. Section 5 presents the results of two studies with different coupling strengths of the voltage to the cytosol calcium. Finally, Section 6 summarizes our conclusions.

2 Dynamics of a Cardiac Cell

In order to understand the electrical excitation, calcium signaling, and mechanical contraction cycle of a cardiomyocyte, it is important to first understand the basic structure of a cardiac cell. A cardiac cell takes the basic shape of a rectangle with T-tubules running along the sides of the cell. The muscle fibers of the cell run parallel with the contractile proteins, which allows for the contraction and relaxation of the cell, represented by links ③ and ④ in Figure 1.1. In Figure 2.1 (a), one can see that a cardiomyocyte contains a sacroplasmic reticulum (SR), which acts as store for calcium ions. The SR contains calcium release units (CRUs), through which calcium is released from the SR to the cytosol of the cell.

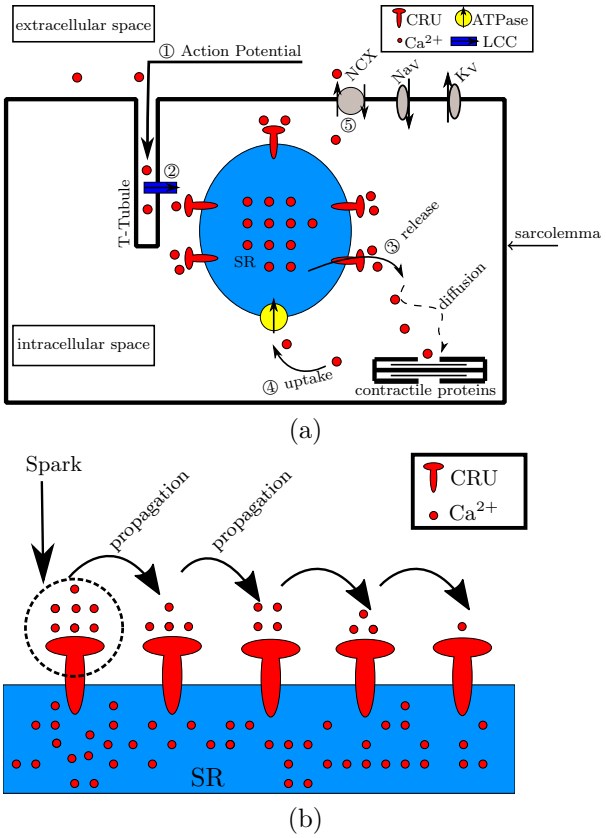

Figure 2.1: (a) Calcium wave triggering. (b) Cascading propagation through cellular space.

Sparking, or the scattered local simultaneous openings of CRUs, occurs when the concentration of calcium is high enough in the cytosol that the CRUs begin to open. In order to see the calcium more easily during experiments, a dye is mixed in the cell's cytosol that will bind to the calcium.

At the top of Figure 2.1 (a), the sodium-calcium electrical exchanger is labeled as NCX. The job of the NCX is to bring three sodium ions into the cell while also pushing out one calcium ion. Link 2 in Figure 1.1 represents this feedback of calcium leaving the cell. The calcium concentration inside the cytosol influences the electrical excitation of this cycle happening inside the cardiomyocyte. As the concentration of calcium in the cytosol begins to change, this causes depolarizations of the cell plasma membrane, which, in turn, causes the action potential that leads to the opening of the L-type Calcium Channels (LCC). This process of action potential causes the LCC to open which is the feedforward mechanism represented as link ① in Figure 1.1. This feedforward mechanism allows for the electrical excitation to influence the calcium concentration in the cytosol. The previously mentioned methods, represented by links ① and ②, lead

to a two-way connection between the electrical excitation and calcium signaling occuring in the cardiac cell.

During the process of calcium release from the CRUs into the cytosol, there exists a spike in calcium concentration which can trigger local CRUs to open in addition to the possible cascading effect illustrated in Figure 2.1 (b). While there is still calcium in the SR, this wave can propagate, then calcium is replenished from an intracellular pump on the SR that acts as a source. Calcium induced calcium release is a behavior described as the process where calcium pours into the cytosol thus increasing the concentration and triggering another wave event within the cell. During calcium diffusion within the cytosol, it reacts with the other chemical species (fluorescent dye, fluoro-4, and tropomyosin contractile proteins).

The contractile proteins, tropomyosin, are responsible for the contraction and expansion of the cell's shape. These proteins are a composition of troponin, actin, myosin heads, and are attached to a sacromere. This sacromere, parallel to the tropomyosin, contracts when the myosin heads come in contact with the actin bridge; this happens when calcium binds to the troponin complex leaving the myosin heads free to converge on the bridge. Myosin contraction can be described as the physical process where the cell expands and contracts; when these contractions perform in unison with other cardiac cells, the corresponding section of the heart pulses. The first coupling between the calcium and the contractile nature of a heart cell is here; we can describe these chemical interactions as a feedforward process and can be represented by link ③ in Figure 1.1. The bridge-like structure deforms once calcium binds to the complex; this causes the bridge to hang onto the calcium longer. The increase in concentration in the cytosol as a feedback process is a result of the calcium being relinquished from the bridge; this process is represented by link ④ in Figure 1.1.

3 Model

This section details the seven variable model used in this work. It is a special case of the eight variable model fully established in [2], obtained by not including all variables so as to focus the simulations on one new effect only. Namely, the full model consists of calcium in the cytosol $c(\mathbf{x},t)$, $n_{sc}=3$ many cytosol buffer species $b_i^{(c)}$, calcium in the SR $s(\mathbf{x},t)$, $n_{ss}=1$ many SR buffer species $b_j^{(s)}$, voltage $V(\mathbf{x},t)$, and the potassium gating function $n(\mathbf{x},t)$. We choose here the number of cytosol buffer species $n_{sc}=3$ in Equation (3.2) and the number of SR buffer species $n_{ss}=0$ in Equation (3.4) in [2]; the value $n_{ss}=0$ indicates that there are no SR buffer species. The seven species of the model are then: calcium in the cytosol $c(\mathbf{x},t)$, a florescent dye $b_1^{(c)}(\mathbf{x},t)$, a contractile protein (troponin) $b_2^{(c)}(\mathbf{x},t)$, a contractile force $b_3^{(c)}(\mathbf{x},t)$, calcium in the SR $s(\mathbf{x},t)$, voltage $V(\mathbf{x},t)$, and the potassium gating function $n(\mathbf{x},t)$. These evolution of these variables are modeled by the system of seven time-dependent, coupled, non-linear reaction diffusion equations

$$\begin{aligned}\frac{\partial c}{\partial t} &= \nabla\cdot(D_c\nabla c)+\sum_{i=1}^{n_{sc}}R_i^{(c)} \\ &\quad+\big(J_{CRU}+J_{leak}-J_{pump}\big) \\ &\quad+\kappa\,J_{LCC}+\big(J_{m_{leak}}-J_{m_{pump}}\big),\end{aligned} \tag{3.1}$$

$$\begin{aligned}\frac{\partial b_i^{(c)}}{\partial t} &= \nabla\cdot(D_{b_i^{(c)}}\nabla b_i^{(c)})+R_i^{(c)}, \\ &\quad i=1,\ldots,n_{sc},\end{aligned} \tag{3.2}$$

$$\begin{aligned}\frac{\partial s}{\partial t} &= \nabla\cdot(D_s\nabla s) \\ &\quad-\gamma(J_{CRU}+J_{leak}-J_{pump}),\end{aligned} \tag{3.3}$$

$$\begin{aligned}\frac{\partial V}{\partial t} &= \nabla\cdot(D_v\nabla V)+\tau_v\,\frac{1}{C}\Big[I_{\text{app}}-g_L(V-V_L) \\ &\quad-g_{Ca}\,m_\infty(V)\,(V-V_{Ca})-g_K\,n\,(V-V_K) \\ &\quad-\omega\,(J_{m_{leak}}-J_{m_{pump}})\Big],\end{aligned} \tag{3.4}$$

$$\begin{aligned}\frac{\partial n}{\partial t} &= \nabla\cdot(D_n\nabla n) \\ &\quad+\tau_v\,\lambda_n\,\cosh\left(\frac{V-V_3}{2V_4}\right)\big(n_\infty(V)-n\big)\end{aligned} \tag{3.5}$$

The following sections provide details on each of the components of the model: Section 3.1 describes the calcium signaling portion of the model. Section 3.2 describes the electrical excitation that is connected to the calcium signaling in both the feedforward and feedback directions represented by link ① and link ② in Figure 1.1. Link ① from electrical system to the calcium dynamics was first established in [1], and link ② was established in [2]. Finally, Section 3.3 presents the mechanical contraction component that is also connected to the calcium signaling in both the feedback and feedforward directions represented by links ③ and ④ in Figure 1.1 and was established in [2].

3.1 Calcium Signaling

The calcium signaling portion of the model consists of the equations (3.1)–(3.3). Table 3.1 collects the variables of the model with their units as well as their initial values. Table 3.2 contains the parameters in the PDEs of the calcium system with their values (if fixed) and units. The coefficients D_c, $D_{b_i^{(c)}}$, and D_s are the diffusivity matrices for Ca^{2+} in the cytosol, buffer species i in the cytosol, and Ca^{2+} in the SR, respectively. While each buffer species programmatically possesses a diffusivity matrix (following the template of (3.2)), not all species are mobile; hence

the diffusivity matrices for some species are zero matrices in Table 3.2.

The reaction terms $R_i^{(c)}$ describe the reactions between calcium and the buffer species. They are the connections between (3.1) and (3.2). More precisely,

$$R_i^{(c)} = -k^+_{b_i^{(c)}}\, c\, b_i^{(c)} + k^-_{b_i^{(c)}} \left(b_{i,total}^{(c)} - b_i^{(c)}\right), \quad i = 1, \ldots, n_{sc}, \tag{3.6}$$

model the reactions between cytosolic Ca^{2+} and each cytosolic buffer species.

In the cytosol, this work considers three buffer species ($n_{sc} = 3$): a fluorescent dye $b_1^{(c)}(\mathbf{x}, t)$, a contractile protein troponin $b_2^{(c)}(\mathbf{x}, t)$, and inactive actin-myosin cross-bridges $b_3^{(c)}(\mathbf{x}, t)$. The reaction model for $b_1^{(c)}(\mathbf{x}, t)$ is (3.6) with $i = 1$ above, but when involving the pseudo-mechanical dynamics of the cell, the reactions for $b_2^{(c)}(\mathbf{x}, t)$ and $b_3^{(c)}(\mathbf{x}, t)$ are in fact given by the modified reaction models (3.18) and (3.17), respectively. This is explained in detail in Section 3.3 below.

Note that in (3.6), ${b_i}^{(c)}$ is the amount of unbound buffer known as "free" buffer. The constant $b_{i,total}^{(c)}$ denotes the total bound and unbound calcium thus leaving the difference seen in (3.6) to be the bound calcium. Since the model uses no-flux boundary conditions, no buffer species escapes or enters the cell, thus we only need to track the "free" buffer species and use $b_{i,total}^{(c)} - {b_i}^{(c)}$ for the bound species.

The flux terms J_{CRU}, J_{leak}, and J_{pump} in (3.1) describe the calcium induced release of Ca^{2+} into the cytosol from the SR, the continuous leak of Ca^{2+} into the cytosol from the SR, and the pumping of Ca^{2+} back into the SR from the cytosol. The terms $J_{LCC}, J_{m_{leak}}$, and $J_{m_{pump}}$ describe the fluxes of calcium into and out of the cell via the plasma membrane. The coupling between (3.1) and (3.3) is achieved by the three flux terms shared by both.

More precisely, J_{LCC}, $J_{m_{leak}}$, and $J_{m_{pump}}$ in (3.1) describe the fluxes of calcium into and out of the cell via the plasma membrane. J_{pump} replenishes the calcium stores in the SR; it increases SR calcium concentration by decreasing cytosol calcium concentration. J_{leak} is a continuous leakage of those SR calcium stores into the cytosol; it increases cytosol concentration by decreasing SR calcium concentration. The pump term

$$J_{pump}(c) = V_{pump}\left(\frac{c^{n_{pump}}}{K_{pump}^{n_{pump}} + c^{n_{pump}}}\right) \tag{3.7}$$

is thus a function of cytosol calcium $c(\mathbf{x}, t)$. The leak term J_{leak} is a constant defined by

$$J_{leak} = J_{pump}(c_0), \tag{3.8}$$

which balances $J_{pump}(c)$ at basal level $c_0 = 0.1\ \mu$M of cytosol calcium. The pump term J_{pump}, a function of cytosolic calcium $c(\mathbf{x}, t)$, consists of the maximum pump velocity V_{pump} multiplied against the relationship between $c(\mathbf{x}, t)$ and the pump sensitivity K_{pump}; the exponent n_{pump} refers to the Hill coefficient (quantifying the degree of cooperative binding) for the pump function. This has the practical effect of multiplying the maximum possible pump velocity against a number between 0 and 1, exclusive. J_{leak}, which continuously leaks calcium into the cytosol from the SR, is simply J_{pump} evaluated at the basal cytosolic calcium concentration $c_0 = 0.1\,\mu M$. As noted, J_{pump} has two roles, namely to balance J_{leak} in the absence of sparking, but also to balance J_{CRU} under conditions of active calcium release.

The term J_{CRU} in (3.1) is the Ca^{2+} flux into the cytosol from the SR via each individual point source at which a CRU has been assigned. The effect of all CRUs is modeled as a superposition such that

$$J_{CRU}(c, s, \mathbf{x}, t) = \sum_{\hat{\mathbf{x}} \in \Omega_s} \hat{\sigma}\, \frac{s(\mathbf{x}, t)}{s_0}\, \mathcal{O}(c, s)\, \delta(\mathbf{x} - \hat{\mathbf{x}}) \tag{3.9}$$

with

$$\mathcal{O}(c, s) = \begin{cases} 1 & \text{if } u_{rand} \le J_{prob}, \\ 0 & \text{if } u_{rand} > J_{prob}, \end{cases} \tag{3.10}$$

where

$$J_{prob}(c, s) = P_{max} \left(\frac{c^{n_{probc}}}{K_{probc}^{n_{probc}} + c^{n_{probc}}}\right)\left(\frac{s^{n_{probs}}}{K_{probs}^{n_{probs}} + s^{n_{probs}}}\right). \tag{3.11}$$

The effect of each CRU is modeled here as a product of three terms: (i) Similarly to how in J_{pump} the maximum pump rate is scaled against the concentration of available cytosol calcium, the maximum pump rate is scaled against the concentration of available cytosol calicum, the maximum rate of Ca^{2+} release $\hat{\sigma}$ is scaled here against the ratio of calcium concentration in the SR. (ii) Following the same pattern a maximum value multiplied against some scaling proportion between 0 and 1 the gating function $\mathcal{O}(c, s)$ has the practical effect of "budgeting" the calcium SR stores such that when the stores are low, the given CRU becomes much less likely to open; each CRU is assigned a uniformly distributed random value, which is compared to the single value returned by the CRU opening probability J_{prob} to determine whether or not the given CRU will open. (iii) The Dirac delta distribution $\delta(\mathbf{x} - \hat{\mathbf{x}})$ models each CRU as a point source for calcium release, which is defined by requiring $\delta(\mathbf{x} - \hat{\mathbf{x}}) = 0$ for all $\mathbf{x} \neq \hat{\mathbf{x}}$ and $\int_{\mathbb{R}^3} \psi(\mathbf{x})\delta(\mathbf{x} - \hat{\mathbf{x}})\, d\mathbf{x} = \psi(\hat{\mathbf{x}})$ for any continuous function $\psi(\mathbf{x})$.

Table 3.1: Variables of the model and their initial conditions. The concentration unit M is shorthand for mol/L (moles per liter).

Variable	Definition	Initial value and units
$\mathbf{x}$	spatial position variable (x, y, z)	μm
t	time variable	ms
$c(\mathbf{x}, t)$	calcium in the cytosol	$c_0 = 0.1$ μM
$b_1^{(c)}(\mathbf{x}, t)$	free flourescent dye in the cytosol	45.918 μM
$b_2^{(c)}(\mathbf{x}, t)$	free troponin in the cytosol	111.818 μM
$b_3^{(c)}(\mathbf{x}, t)$	inactive actin-myosin cross-bridges [X] in the cytosol	145.20 μM
$s(\mathbf{x}, t)$	calcium in the SR	$s_0 = 10{,}000$ μM
$V(\mathbf{x}, t)$	membrane potential (voltage)	-50 mV
$n(\mathbf{x}, t)$	fraction of open potassium channels	0.1

3.2 Electrical Excitation

The calcium signaling portion of the model consists of the equations (3.4)–(3.5). The membrane potential of the cell depends on both the cytosol calcium ion concentration and also on the cytosol potassium ion (K^+) concentration [3, 8]. In our model, the ω term in (3.4) quantifies a dependence of V on c to complete the coupling from the chemical to the electrical systems in link ② in Figure 1.1 [2], after c in (3.1) already contains several terms that depend on V to implement link ① in Figure 1.1. Table 3.3 contains the variables and parameters for electrical excitation. The Ca^{2+} conductance is much faster than the K^+ conductance, so the calcium conductance can be approximated as m_∞ or instantaneously steady-state at all times; the potassium conductance requires a separate description in (3.5) Needed parameter functions in (3.4)–(3.5) are

$$m_\infty(V) = \frac{1}{2}\left(1 + \tanh\left(\frac{V - V_1}{V_2}\right)\right), \tag{3.12}$$

$$n_\infty(V) = \frac{1}{2}\left(1 + \tanh\left(\frac{V - V_3}{V_4}\right)\right). \tag{3.13}$$

The connection between (3.1) and (3.4), link ① in Figure 1.1, the link from the electrical system to the calcium system, comes through

$$J_{LCC} = \frac{\tau_{flux}}{2F}\, S\, g_{Ca}\, m_\infty(V)\,(V - V_{Ca}), \tag{3.14}$$

the only calcium flux term to involve voltage. Note the parameter κ in (3.1), which is an external scaling factor for J_{LCC} rather than an intrinsic physiological component; if the value of κ is set to 0, the connection, link ① in Figure 1.1, is effectively switched off and the calcium dynamics are then modeled as though voltage were not involved. The surface area, S, of the cell is included in light of the fact that J_{LCC} describes the influx of calcium through L-type calcium channels (LCCs), which are present in the enclosing plasma membrane of the cell: the surface area of the cell is the surface area of the membrane.

We model the effect of the cytosol calcium concentration on the voltage by treating the calcium efflux term $(J_{m_{pump}} - J_{m_{leak}})$ as equivalent to the sodium-calcium exchanger current: we are thus able to describe the current generated by the sodium-calcium exchange as a function of simple calcium loss.

The individual components of the calcium efflux term are near-duplicates in form of the earlier J_{pump} and J_{leak} functions in (3.7) and (3.8), respectively. As J_{pump} described the removal of calcium from the cytosol and its transfer into SR stores,

$$J_{m_{pump}}(c) \;=\; V_{m_{pump}}\left(\frac{c^{n_{mpump}}}{K_{m_{pump}}^{n_{mpump}} + c^{n_{mpump}}}\right) \tag{3.15}$$

describes the removal of calcium from the cytosol and its transfer to outside the cell across the membrane. The leak term J_{leak} described a gradual leak of calcium into the cytosol from the SR, while J_{CRU} described an abrupt, high-concentration (high relative to the leak) release of calcium into the cytosol from the SR. Similarly,

$$J_{m_{leak}} \;=\; J_{m_{pump}}(c_0) \tag{3.16}$$

describes a gradual leak of calcium into the cytosol from outside the cell via the plasma membrane, while J_{LCC} describes a sudden spike of calcium release into the cytosol via the LCCs.

The model connects the chemical system to the electrical system, link ② in Figure 1.1, via the inclusion of the current generated by calcium leaving the cell via $J_{m_{pump}}$ and $J_{m_{leak}}$, which directly affects the voltage. We collect and incorporate these as a single term, the calcium efflux $(J_{m_{pump}} - J_{m_{leak}})$, and use ω in (3.4) as a parameter for feedback strength in link ② in Figure 1.1, which is a scaling factor with the same essential function as κ in link ①

Table 3.2: Parameters for calcium signaling.

Variable	Definition	Values/Units
D_c	diffusivity matrix for $c(\mathbf{x},t)$	diag(0.15,0.15,0.3) μm^2/ms
$D_{b_1^{(c)}}$	diffusivity matrix for $b_1^{(c)}$	diag(0.01,0.01,0.02) μm^2/ms
$D_{b_2^{(c)}}$	diffusivity matrix for $b_2^{(c)}$	diag(0.00,0.00,0.00) μm^2/ms
$D_{b_3^{(c)}}$	diffusivity matrix for $b_3^{(c)}$	diag(0.00,0.00,0.00) μm^2/ms
D_s	diffusivity matrix for $s(\mathbf{x},t)$	diag(0.78,0.78,0.78) μm^2/ms
$R_i^{(c)}$	reactions of cytosol Ca^{2+} with buffers	μM/ms
$k^+_{b_1^{(c)}}$	forward reaction coefficient for $b_1^{(c)}$	0.080 (μM ms)$^{-1}$
$k^+_{b_2^{(c)}}$	forward reaction coefficient for $b_2^{(c)}$	0.100 (μM ms)$^{-1}$
$k^+_{b_3^{(c)}}$	forward reaction coefficient for $b_3^{(c)}$	0.040 ms^{-1}
$k^-_{b_1^{(c)}}$	reverse reaction coefficient for $b_1^{(c)}$	0.090 ms^{-1}
$k^-_{b_2^{(c)}}$	reverse reaction coefficient for $b_2^{(c)}$	0.100 ms^{-1}
$k^-_{b_3^{(c)}}$	reverse reaction coefficient for $b_3^{(c)}$	0.010 ms^{-1}
$b^{(c)}_{1,total}$	total amount of $b_1^{(c)}$ in the cytosol	50 μM
$b^{(c)}_{2,total}$	total amount of $b_2^{(c)}$ in the cytosol	123 μM
$b^{(c)}_{3,total}$	total amount of $b_3^{(c)}$ in the cytosol	150 μM
γ	ratio of volume of cytosol to SR	14
J_{leak}	calcium leak from SR	0.3209684 μM/ms
J_{pump}	calcium transfer from cytosol to SR	μM/ms
V_{pump}	maximum pump rate	4 μM/ms
K_{pump}	pump sensitivity to Ca^{2+}	0.184 μM
n_{pump}	Hill coefficient for pump function	4.0
J_{CRU}	calcium flux from SR to cytosol via CRUs	μM/ms
$\mathcal{O}$	gating function for J_{CRU}	0 or 1
J_{prob}	probability of CRU opening	0 to 1
$\mathbf{x}_s$	three-dimensional vector for CRU location	μm
Δx_s, Δy_s, Δz_s	CRU spacings in x-, y-, z-directions	0.8, 0.8, 2.0 μm
$\hat{\sigma}$	maximum rate of release	200 μM μm^3/ms
$\delta(\mathbf{x}-\hat{\mathbf{x}})$	Dirac delta distribution	$1/\mu$m^3
u_{rand}	uniformly distributed random variable	0 to 1
P_{max}	maximum probability for release	0.3
K_{prob_c}	sensitivity of CRU to cytosol calcium	2 μM
n_{prob_c}	Hill coefficient for probability function	4
K_{prob_s}	sensitivity of CRU to SR calcium	550 μM
n_{prob_s}	Hill coefficient for probability function	4

Table 3.3: Parameters for electrical excitation and mechanical contraction with base units of mho = $(s^3A^2)/(kg\ m^2)$ and F = $(s^4A^2)/(kg\ m^2)$.

Variable	Definition	Values/Units
D_v	diffusivity matrix for $V(\mathbf{x},t)$	diag(0.00,0.00,0.00) $\mu m^2/ms$
D_n	diffusivity matrix for $n(\mathbf{x},t)$	diag(0.00,0.00,0.00) $\mu m^2/ms$
τ_v	scaling factor to fit action potential duration in voltage equation	0.1 μM μm^3/ms
τ_{flux}	scaling factor to fit action potential duration in J_{LCC} equation	0.1
V_1	potential at which $m_\infty = 0.5$	-1.0 mV
V_2	reciprocal of slope of voltage dependence of m_∞	15.0 mV
V_3	potential at which $n_\infty = 0.5$	10.0 mV
V_4	reciprocal of slope of voltage dependence of n_∞	14.5 mV
V_L	equilibrium potential for leak conductance	-50 mV
V_{Ca}	equilibrium potential for Ca^{2+} conductance	100 mV
V_K	equilibrium potential for K^+ conductance	-70 mV
C	membrane capacitance	20 $\mu F/cm^2$
I_{app}	applied current	50 $\mu A/cm^2$
g_L	maximum/instantaneous conductance for leak	2 mmho/cm^2
g_{Ca}	maximum/instantaneous conductance for Ca^{2+}	4 mmho/cm^2
g_K	maximum/instantaneous conductance for K^+	8 mmho/cm^2
m_∞	fraction of open calcium channels at steady state	0 to 1
n_∞	fraction of open potassium channels at steady state	1
λ_n	maximum rate constant for opening of K^+ channels	0.1 ms^{-1}
J_{LCC}	influx of calcium into cell via L-type calcium channels	μM/ms
S	surface area of the cell	3604.48 μm
F	Faraday constant	95484.56 C/mol
κ	scaling factor of J_{LCC}	0.01 or 0.1
ω	feedback strength (scaling factor) for Ca^{2+} efflux	μA ms/μM cm^2
$J_{m_{leak}}$	leak of calcium out from cell via L-type calcium channels	0.1739493 μM/ms
$J_{m_{pump}}$	pump of calcium out from cell via L-type calcium channels	μM/ms
$V_{m_{pump}}$	maximum pump rate	2 μM/ms
$n_{m_{pump}}$	membrane pump Hill coefficient	4
$K_{m_{pump}}$	membrane pump Ca^2+ sensitivity	0.18
$[XB]_0$	initial concentration of active cross-bridges	142.6805 μM
ε	shortening factor	0 to 1
F_{max}	maximum force generated by actin-myosin crossbridges	10 μN
k_s	stiffness of actin filament	0.025 N/m

in Figure 1.1 from (3.1): if it is set to 0, the only terms of (3.4) which depend on the cytosolic calcium concentration drop out, and the connection from calcium signaling to electrical excitation is severed.

3.3 Pseudo-Mechanical Contraction

The links ③ and ④ in Figure 1.1 provide feedback and feedforward terms for the contractile dynamics. We describe this as "pseudo-mechanical" because the domain itself is unchanged; in our model, the physical dimensions of the cell and the locations of the CRUs do not change. We instead model the contraction via the proportion of contractile proteins which have bound to calcium and changed shape as a result, which generates the force required for cell contraction. Table 3.3 contains the parameters for pseudo-mechanical contraction.

The contractile proteins in question, though considered as a single species, are the combination of actin and myosin when linked via cross-bridges. This linkage is made possible by Ca^{2+} binding to troponin, the cytosol buffer species $b_2^{(c)}(\mathbf{x},t)$: it is this binding that allows the actin-myosin cross-bridges to form. The cytosol species, $b_3^{(c)}(\mathbf{x},t)$, describes these actin-myosin cross-bridges and constructs a third cytosol reaction term

$$R_{b_3}^{(c)} = -k^+_{b_3^{(c)}} \left(\frac{b_{2,total}^{(c)} - b_2^{(c)}}{b_{2,total}^{(c)}} \right)^2 b_3^{(c)} + k^-_{b_3^{(c)}} (b_{3,total}^{(c)} - b_3^{(c)}). \quad (3.17)$$

Notice that this is not the same as the generic pattern for buffer species reaction terms from the initial model. There is no immediately clear dependence on cytosolic calcium $c(\mathbf{x},t)$. However, while $c(\mathbf{x},t)$ is not explicitly included, it is present in the proportion involving troponin, $b_3^{(c)}(\mathbf{x},t)$, which itself depends explicitly on cytosol calcium levels; $R_{b_3}^{(c)}$, like the other two reaction equations, does in fact depend on cytosol calcium concentration.

When troponin binds to Ca^{2+}, the protein as a whole changes shape: this not only allow actin-myosin cross-bridges to form, but also traps the calcium in its connection to the troponin so that the disassociation rate decreases dramatically. To account for this, the shortening factor ε describes how the separation of troponin and calcium has been physically, but not chemically, impaired. Note, again, that $R_{b_2}^{(c)}$ remains a function of cytosol calcium concentration $c(\mathbf{x},t)$ by its equation

$$R_{b_2}^{(c)} = -k^+_{b_2^{(c)}} c\, b_2^{(c)} + k^-_{b_2^{(c)}} \left(b_{2,total}^{(c)} - b_2^{(c)} \right) \frac{1}{\varepsilon} \quad (3.18)$$

with

$$\varepsilon = \exp\left(F_{max}\, k_s \left(\frac{b_{3,total}^{(c)} - b_3^{(c)} - [XB]_0}{b_{3,total}^{(c)} - [XB]_0} \right) \right) \quad (3.19)$$

and

$$[XB]_0 = b_{3,total}^{(c)} - b_3^{(c)}(\mathbf{x},0). \quad (3.20)$$

This shortening factor ε links ③ and ④ in Figure 1.1. It refers back to the concentration of $b_3^{(c)}(\mathbf{x},t)$, the actin-myosin cross-bridges, and to the force that their linkage generates. It is scaled by the maximum possible contractile force F_{max}, the actin stiffness k_s, and the proportion of active to inactive actin-myosin cross-bridges.

The force in the cell is generated by the bound cross-bridge. While assuming a linear relationship between the force that the bound cross bridge produces and the concentration of the bound cross-bridge, this force can be represented by the following equation:

$$F = F_{max} \frac{(b_{3,total}^{(c)} - b_3^{(c)}) - (b_{3,total}^{(c)} - b_3^{(c)}(\mathbf{x},0))}{b_{3,total}^{(c)} - (b_{3,total}^{(c)} - b_3^{(c)}(\mathbf{x},0))}. \quad (3.21)$$

Like ω and κ, the factor ε is our point of control over the linkage between systems: if the argument of the exponential function is 0, the overall value simply turns to 1, and $R_{b_2}^{(c)}$ in (3.18) reverts to its earlier form (3.6) with $i = 2$.

These two reaction terms (3.17) and (3.18) connect the three components of our model. The calcium signaling is linked to the pseudo-mechanical contraction through the cross-bridge term, and the pseudo-mechanical contraction is in turn connected to the calcium signaling through the inclusion of the cytosol calcium concentration in the modified reaction equation for troponin. Thus all links ①, ②, ③, and ④ in Figure 1.1 are established, and thus the three systems of the model are fully linked.

3.4 Initial and Boundary Conditions

The concentration of cytosol calcium $c(\mathbf{x},0)$ is initialized to its basal level $c_0 = 0.1$ μM throughout the cell.

The initial values of all three cytosol buffer species $b_i^{(c)}(\mathbf{x},0)$, $i = 1,2,3$, in the model are chosen such that their reaction rates $R_i^{(c)} = 0$ when cytosol calcium is at basal level. Thus, it is not reactions that will prompt changes in the simulations after the initial time.

Specifically, $b_1^{(c)}(\mathbf{x},0)$ at time $t = 0$ is calculated by setting $R_i^{(c)}$ with $i = 1$ in (3.6) to 0. With $c(\mathbf{x},0) = 0.1$ μM, this yields

$$b_1^{(c)}(\mathbf{x},0) = \frac{k^-_{b_1^{(c)}} b_{1,total}^{(c)}}{k^+_{b_1^{(c)}} c_0 + k^-_{b_1^{(c)}}} \quad (3.22)$$

as formula for $b_1^{(c)}$ at the initial time.

Before setting $R_2^{(c)}$ to 0 to find a formula for $b_2^{(c)}(\mathbf{x},0)$, we note first two facts: (i) By definition $b_3^{(c)}(\mathbf{x},0) + [XB]_0 = b_{3,total}^{(c)}$, that is, the sum of $b_3^{(c)}$ at the initial time plus $[XB]_0$ equals their combined maximum. (ii) Thus, at time $t = 0$, the numerator in the $\exp(\cdot)$ function in (3.19) is 0 and thus the shortening factor ε in (3.19) has value 1.0 initially. Thus, the modified $R_2^{(c)}$ in (3.18) collapses to (3.6) with $i = 2$, and solving $R_2^{(c)} = 0$ yields

$$b_2^{(c)}(\mathbf{x},0) = \frac{k^-_{b_2^{(c)}} b_{2,total}^{(c)}}{k^+_{b_2^{(c)}} c_0 + k^-_{b_2^{(c)}}}. \tag{3.23}$$

This equation involves again the basal level $c_0 = c(\mathbf{x},0)$, but does not involve $b_3^{(c)}$, hence it can be computed first.

In order to find the initial value of $b_3^{(c)}(\mathbf{x},0)$, we set $R_{b_3}^{(c)}$ from (3.17) to 0. With $b_2^{(c)}(\mathbf{x},0)$ computed first from (3.23) above, it can be used here and solving $R_{b_3}^{(c)} = 0$ leads then to the computable formula

$$b_3^{(c)}(\mathbf{x},0) = \frac{k^-_{b_3^{(c)}} b_{3,total}^{(c)}}{k^+_{b_3^{(c)}} \left(\frac{b_{2,total}^{(c)} - b_2^{(c)}(\mathbf{x},0)}{b_{2,total}^{(c)}} \right)^2 + k^-_{b_3^{(c)}}}. \tag{3.24}$$

The definition $b_3^{(c)}(\mathbf{x},0) + [XB]_0 = b_{3,total}^{(c)}$ is then used to compute the value (3.20) for use in (3.19).

The value $s_0 = 10{,}000$ μM is chosen as the initial concentration for the store $s(\mathbf{x},0)$ of calcium in the SR throughout the cell. This choice represents a high value for the store of calcium in the SR, so that this is not a limiting factor to CRU activation initially.

For the variables in the electrical part of the model, we use $V(\mathbf{x},0) = -50$ mV for the membrane potential and $n(\mathbf{x},0) = 0.1$ for the fraction of open potassium channels.

The model uses no-flow boundary conditions for all diffusive variable, thus containing the total number of molecules of each species inside the cell.

4 Numerical Method

In order to do calculations for the CICR model, we need to solve the system of time-dependent parabolic partial differential equations (PDEs) specified in Section 3. The PDEs are coupled by several non-linear reaction, source, and other terms on the right-hand side of the PDEs. For the simulations in Section 5, we have the seven variables specified in Table 3.1, thus we have $n_s = 7$ coupled PDEs. The domain in our model is a hexahedron $\Omega = (-6.4, 6.4) \times (-6.4, 6.4) \times (-32.0, 32.0)$ in units of μm with isotropic CRU distribution that captures the key feature of the elongated shape of a heart cell.

We take a method of lines (MOL) approach to spatially discretize this model, with the finite volume method (FVM) as the spatial discretization with $(N_x + 1)$, $(N_y + 1)$, $(N_z + 1)$ control volumes in the x-, y-, z-coordinate directions, thus there are a total of $N = (N_x + 1)(N_y + 1)(N_z + 1)$ control volumes. The simulations in Section 5 use $N_x = N_y = 32$ and $N_z = 128$. Applying this to the case of the $n_s = 7$ PDEs results in a large system of ordinary differential equations (ODEs) with $n_{eq} = n_s N = 983{,}367$ degrees of freedom (DOF) as size of the system that needs to be solved at every time step.

A MOL discretization of a diffusion-reaction equations with second-order spatial derivatives results in a stiff ODE system. The time step size restrictions, due to the CFL condition, are considered too severe to allow for explicit time-stepping methods. This necessitates the use of a sophisticated ODE solver such as the family of numerical differentiation formulas (NDFk). Stiff ODEs need an implicit ODE method, thus requiring the solution of a non-linear system at every time step. We use the Newton method as non-linear solver, and the linear system in each Newton step is solved by BiCGSTAB as the linear solver. Complete details of the numerical method can be found in [5, 10], and [4] contains practical details for the implementation, specifically the analytical derivation of the Jacobian matrix that is required for optimal convergence of the Newton method. BiCGSTAB is a Krylov subspace method, which only requires matrix-vector products with the system matrix, not the matrix itself. Thus, we can dramatically reduce memory usage by using a matrix-free implementation of the linear solver that does not store the system matrix, but provides the results of the matrix-vector product. The code with the NDFk method of orders $1 \le k \le 5$ requires then, including all auxiliary method vectors, the storage of only 17 arrays of significant size n_{eq}.

The implementation of the model uses C and MPI to parallelize computations. Parallelization is accomplished by block-distributing all large arrays to all MPI processes with split along the long z-direction. MPI commands `MPI_Isend` and `MPI_Irecv` are non-blocking point-to-point communication commands used to communicate the interface data between blocks on neighboring processes. The collective command `MPI_Allreduce` is used in the computation of scalar products and norms.

Runs were done on maya in the UMBC High Performance Computing Facility (HPCF). The components used from the cluster are the 72 nodes with two eight-core 2.6 GHz Intel E5-2650v2 Ivy Bridge CPUs and 64 GB memory. The nodes are connected by a high-speed quad-data rate (QDR) InfiniBand network. Using 8 nodes of this machine, the runs typically took between ten minutes and thirty minutes per run with the times being largely dependent on the number of time steps.

5 Results

This section shows the results of simulations for the seven variable model detailed in Section 3. Specifically, Subsections 5.1 and 5.2 consider different strengths of the linkage of the voltage system to the cytosol calcium by parameter κ in Equation (3.1): Subsection 5.1 considers a higher coupling strength of $\kappa = 0.1$ and Subsection 5.2 a lower coupling strength of $\kappa = 0.01$.

The following figures focus on the four most instructive variables c, ${b_3}^{(c)}$, s, and V from (3.1)–(3.5) plus plots of open calcium release units; the technical report [4] includes results for all seven variables, but we only report on those here that exhibit a notable difference for the values of coupling strenghts considered.

5.1 Higher Coupling Strength $\kappa = 0.1$

This subsection contains Figures 5.1 through 5.5, based on simulations using the values in Tables 3.1, 3.2, and 3.3, and coupling strength $\kappa = 0.1$.

Figure 5.1 (a) plots the voltage in mV measured at the center point of the cell against time in ms in order to show how the voltage changes over the 1,000 ms time period. The voltage is the driving force for all other events happening in the cell. Voltage is represented by Equation (3.4) and is responsible the electrical excitation component of the model in Figure 1.1. This excitation is communicated through the J_{LCC} term in Equation (3.1), whose strength is controlled by κ.

The plots in Figure 5.2 display the locations of open calcium release units by a dot. The more dark dots are visible, the more CRUs are open at that specific time. At some times and for short periods of time, CRUs form patterns and initiate diffusion waves, but no sustained waves form that would move through the entire cell. When many dark dots appear in an unorganized uniformly distributed fashion across the cell domain, this represents spontaneous sparking within the cell. The opening of CRUs is controlled by the model in Equations (3.9)–(3.11). This model embodies the effect of Calcium Induced Calcium Release (CICR) into the cytosol in that a higher concentration of cytosol calcium increases the probability for a CRU to open in (3.11), and an open CRU in turn increases the cytosol calcium concentration through the term J_{CRU} in Equation (3.1). Notice that the original trigger for increasing cytosol calcium comes from the J_{LCC} term in Equation (3.1) controlled by the voltage.

Figure 5.3 shows a collection of isosurface plots for calcium concentration in the cytosol. An isosurface plot displays the surface in the three-dimensional cell, where the species concentration is equal to a critical value, stated in the caption of the figure, here 65 μM for the concentration of cytosol calcium $c(\mathbf{x}, t)$. Due to the connection with open CRUs through the effect of Calcium Induced Calcium Release, calcium concentration in the cytosol in Figure 5.3 is high in the same areas of the cell where the CRUs are open in Figure 5.2 at that time.

Figure 5.4 represents the concentration of the inactive actin-myosin cross-bridges throughout the cell, modeled by Equation (3.17). The plots indicates that at locations and times of increased cytosol calcium concentrations in Figure 5.3, the concentration of the *inactive* bridges decreases in Figure 5.4, implying an increase in the *active* bridges. These values enter into Equation (3.19) for the shortening factor ε, whose values decrease from the neutral value 1.0 in these conditions. The plot of ε at the center of the cell in Figure 5.1 (b) shows this behavior and indicates the connection to mechanical contraction component in Figure 1.1.

The plots displaying the calcium concentration $s(\mathbf{x}, t)$ of the store in the SR are located in Figure 5.5. The store in the SR has an initial value of 10,000 μM. When comparing these plots to the plots of calcium in the cytosol in Figure 5.3, we can see that there is a relationship. As the calcium concentration in the cytosol increases, more CRUs open as seen in Figure 5.2, which releases more calcium from the SR into the cytosol, resulting in a decreased concentration of the store in the SR. This is the effect of the J_{CRU} term with a negative sign in Equation (3.3) for $s(\mathbf{x}, t)$. A decreased value of $s(\mathbf{x}, t)$ at a certain location is of interest, since this limits eventually the ability of the CRU at that location to open in (3.11) as well as limits the amount of calcium released through the CRU in (3.9). We notice that due to more spontaneous openings of CRUs in the right end of the cell, the store concentration shows a larger decrease there.

Finally, Figure 5.1 (b) plots the shortening factor ε in (3.19) against time to show how the shortening factor changes over time. After comparing Figure 5.1 (b) to Figure 5.1 (a), we can see that the shortening factor mirrors the voltage plot such that as voltage increases, the shortening factor decreases. Likewise, as the voltage decreases, the shortening factor increases. This shows that the voltage is the driving force between the contraction and relaxation of a heart cell.

5.2 Lower Coupling Strength $\kappa = 0.01$

This subsection contains Figures 5.6 through 5.10, based on simulations using the values in Tables 3.1, 3.2, and 3.3, and coupling strength $\kappa = 0.01$.

After comparing Figures 5.1 (a) and 5.6 (a), there is no noticable change between the voltage when $\kappa = 0.1$ versus when $\kappa = 0.01$. This means that the voltage as driver of the process is not strongly influenced by the coupling of the system's components. This makes sense, since κ is

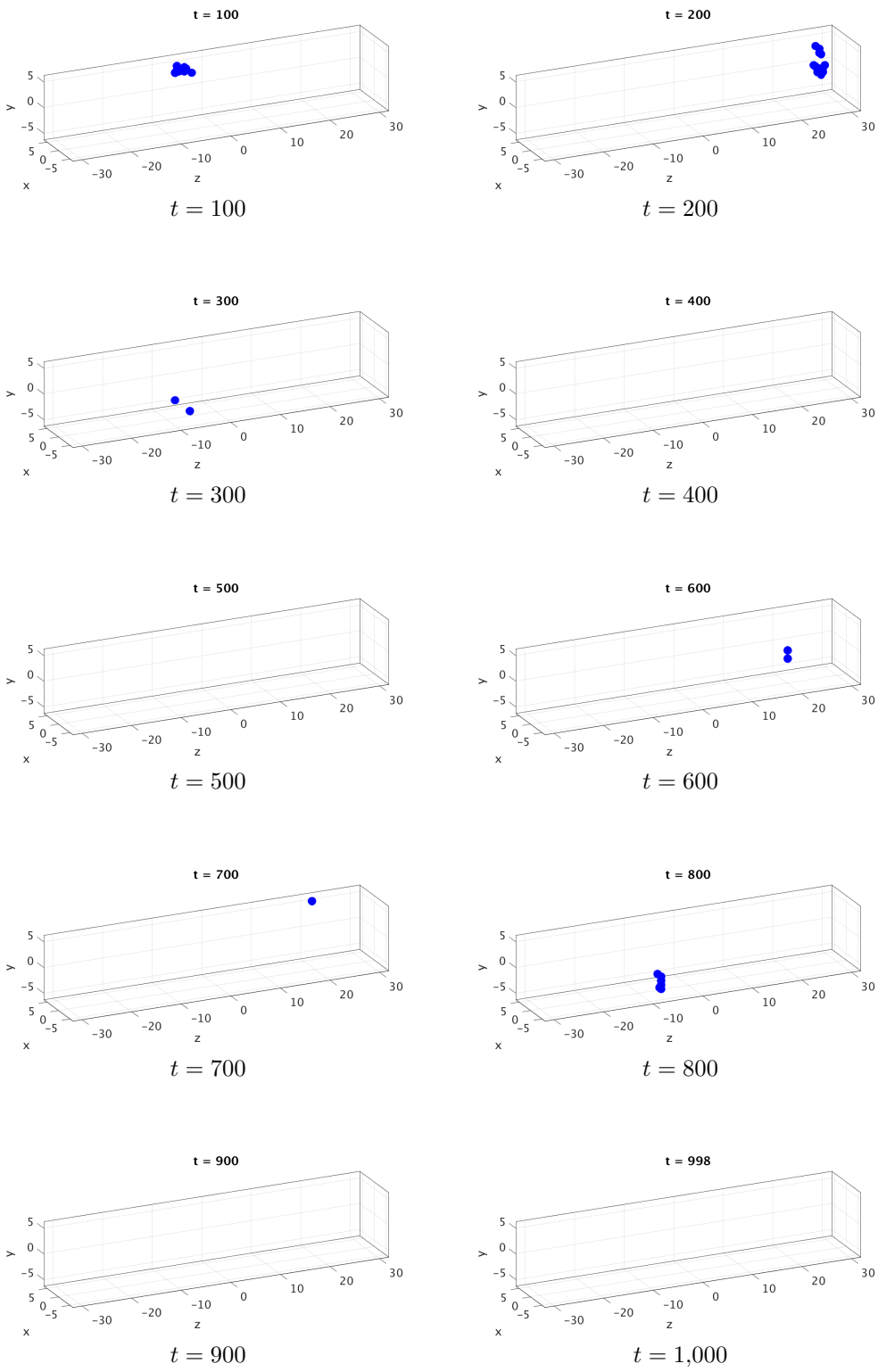

Figure 5.2: Open calcium release units throughout the cell for $\kappa = 0.1$.

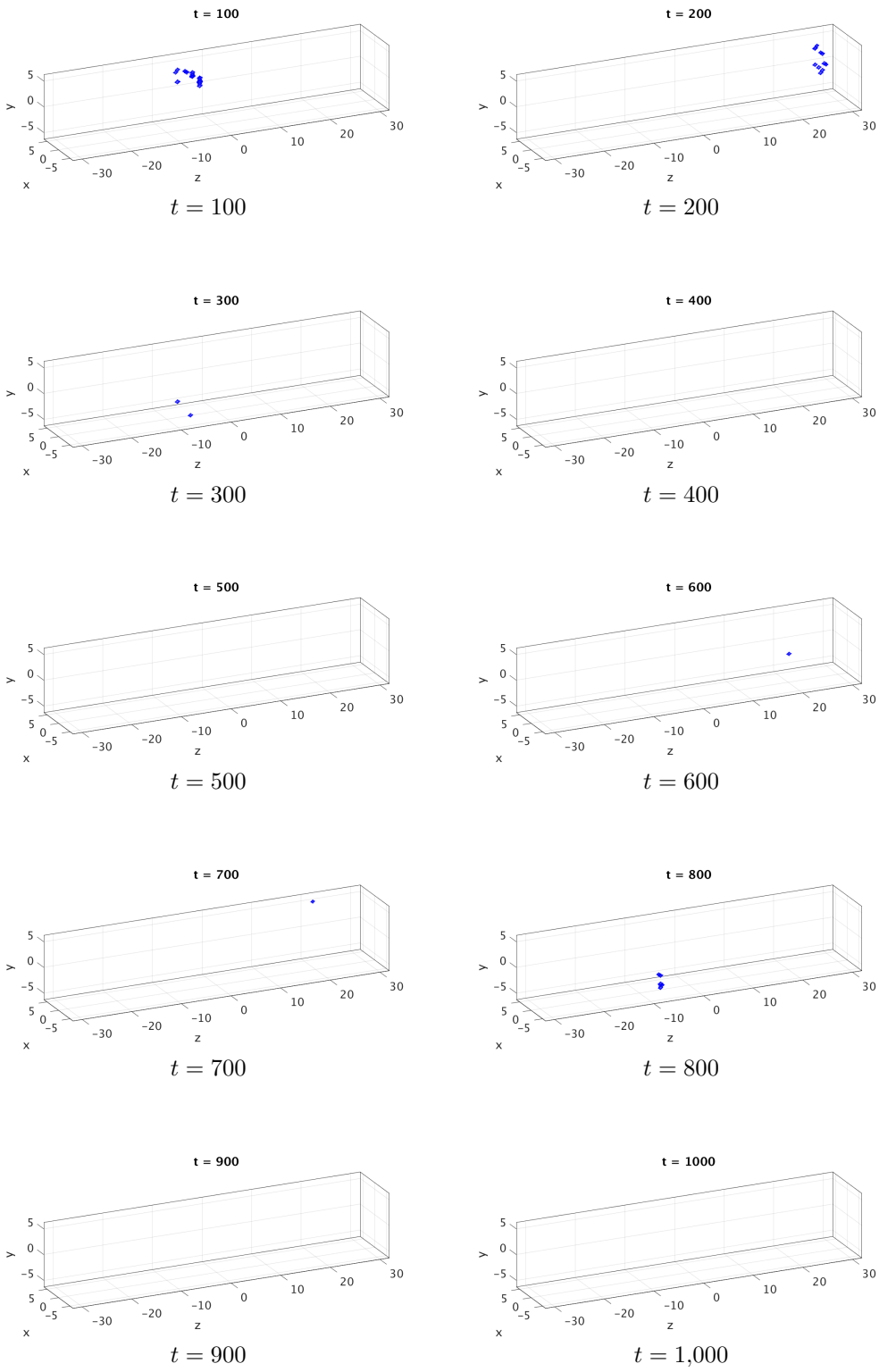

Figure 5.3: Concentration of $c(\mathbf{x}, t)$ throughout the cell for $\kappa = 0.1$, with a critical value of 65 μM.

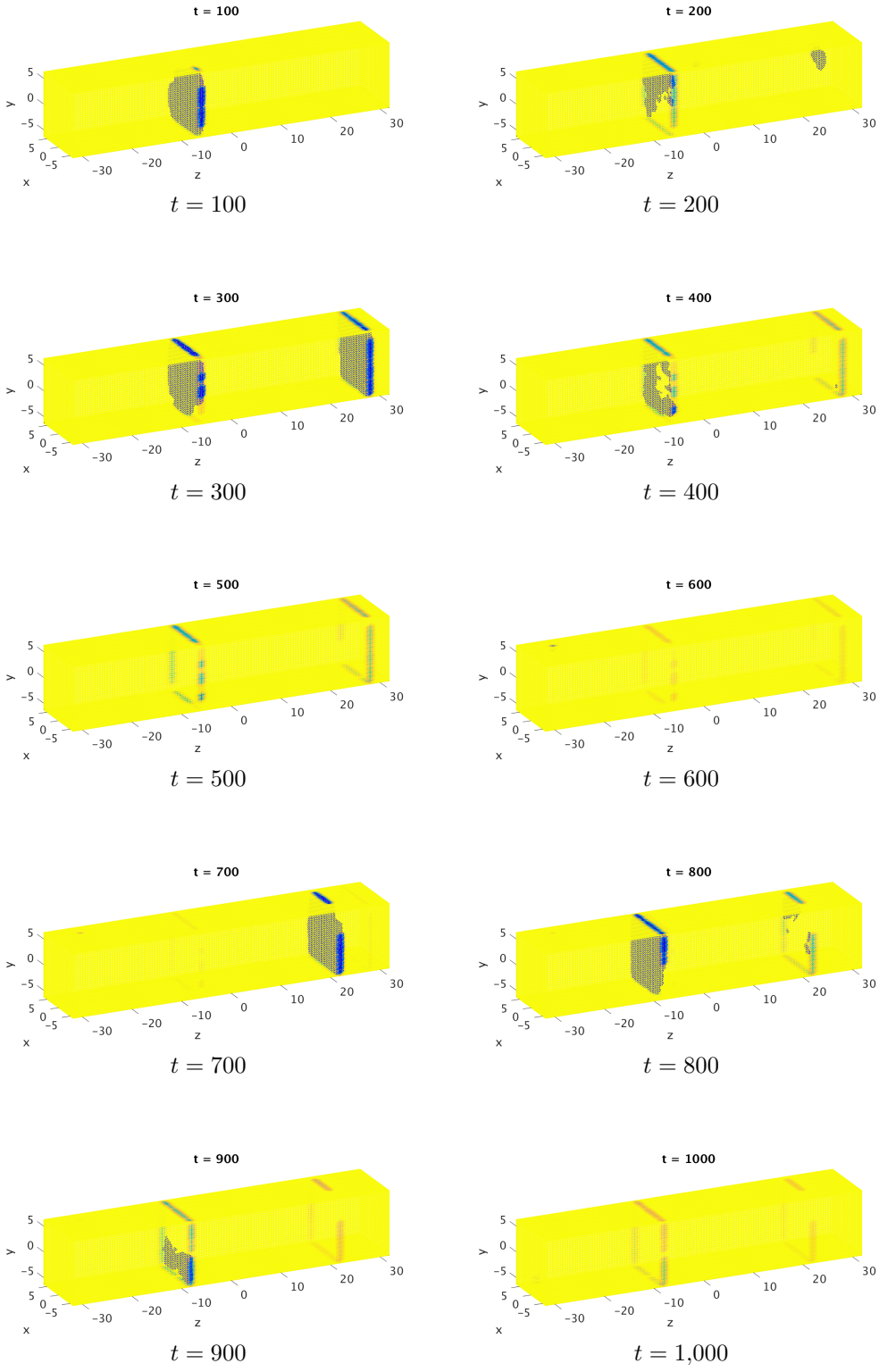

Figure 5.4: Concentration of ${b_3}^{(c)}(\mathbf{x}, t)$ throughout the cell for $\kappa = 0.1$, with a critical value of 120 μM.

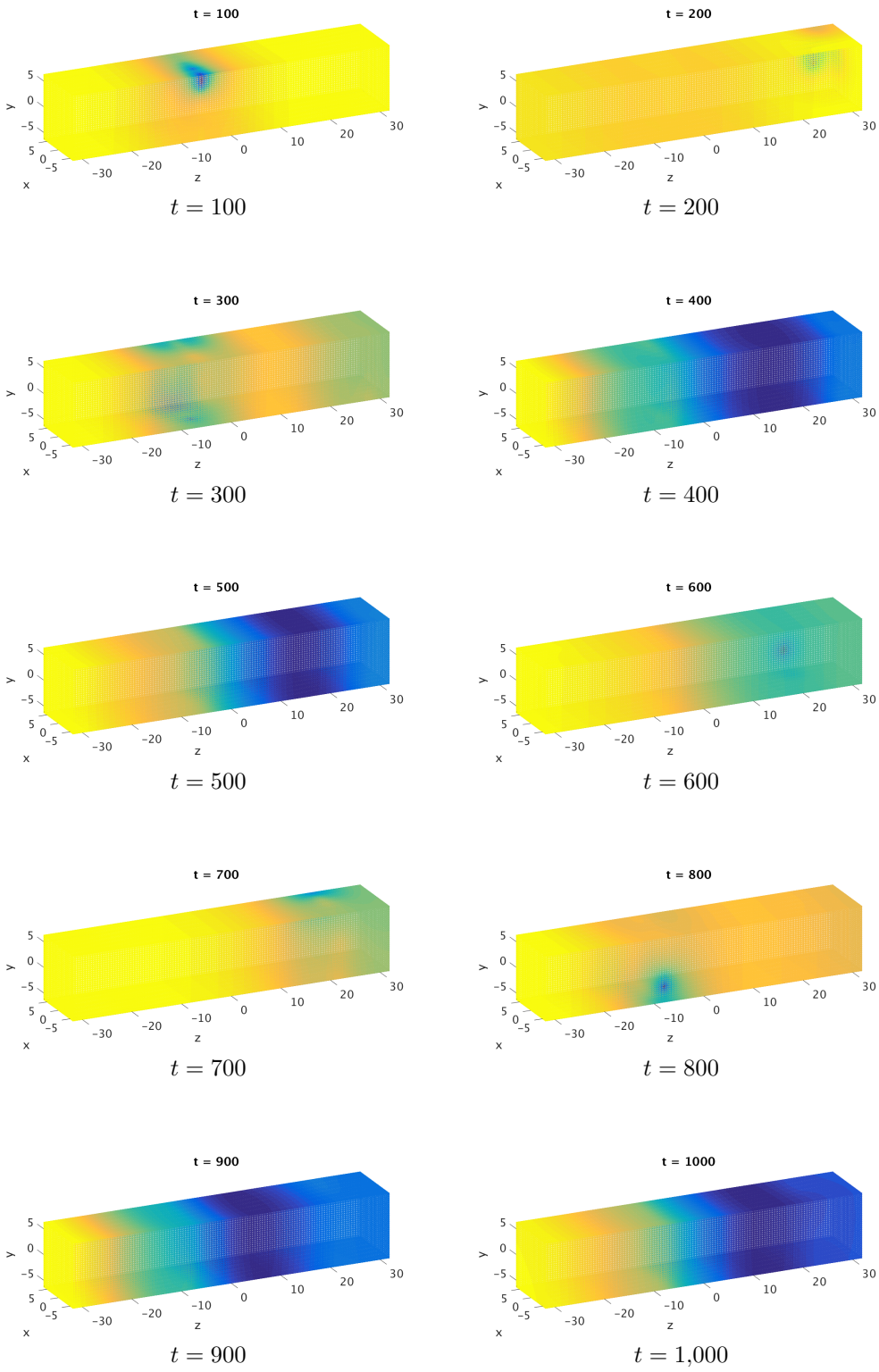

Figure 5.5: Concentration of $s(\mathbf{x}, t)$ throughout the cell for $\kappa = 0.1$, with a critical value of 5,000 μM.

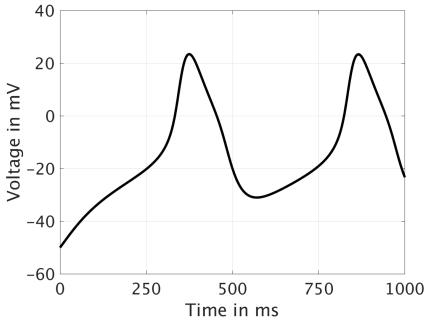

(a) Voltage vs. time

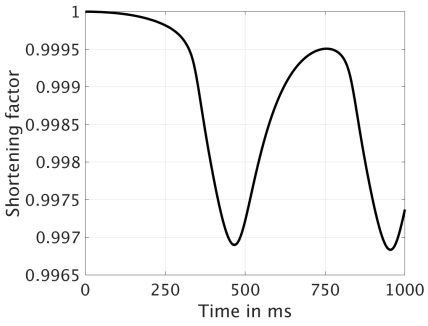

(b) Shortening factor vs. time

Figure 5.1: Voltage and shortening factor vs. time for $\kappa = 0.1$.

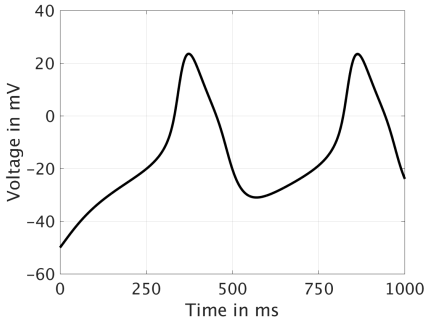

(a) Voltage vs. time

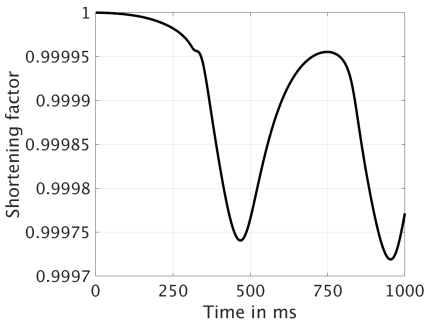

(b) Shortening factor vs. time

Figure 5.6: Voltage and shortening factor vs. time for $\kappa = 0.01$.

in (3.1) and V in (3.4) is only very indirectly affected by changes in κ. Recall that we are not prescribing V, but the results in Figures 5.1 (a) and 5.6 (a) simply emerge from the simulations of the coupled PDEs and their initial conditions.

When comparing Figures 5.3 and 5.8, we can see that the calcium concentration in the cytosol is slightly more active when $\kappa = 0.01$ than when $\kappa = 0.1$. So, a *stronger* coupling results in *less* change in c, i.e., smaller derivatives $\partial c/\partial t$. This makes sense when noting that the term J_{LCC} in (3.14) is negative for $V = -50$ mV, which is the initial value of V. Only when V becomes positive and sufficiently large at a later time, see Figures 5.1 (a) and 5.6 (a), the effect reverses, since eventually J_{LCC} becomes positive then.

It is also evident that there is a change in the mechanical component of the model with a change in the value of κ when looking at Figures 5.4 and 5.9. For example, when $\kappa = 0.01$, there are less inactive actin-myosin cross-bridges during a significant portion of the 1,000 milliseconds shown in Figure 5.9 than in Figure 5.4 for $\kappa = 0.1$. This is evident by an increase of dark sections in the plots in Figure 5.9 compared to Figure 5.4. This shows that more actin-myosin cross-bridges are becoming activated in the $\kappa = 0.01$ case.

We can also see differences between the calcium concentration in the store in the SR when $\kappa = 0.1$ versus when $\kappa = 0.01$, as evident by comparing Figures 5.5 and 5.10. For example, the SR displays a larger depletion of calcium at time $t = 500$ ms for $\kappa = 0.1$ in Figure 5.5 compared to $t = 500$ ms for $\kappa = 0.01$ in Figure 5.10. Differences continue to appear at various times between these two cases.

Finally, while the plots of the shortening factor over time look very similar for cases $\kappa = 0.1$ and $\kappa = 0.01$ in Figures 5.1 (b) and 5.6 (b), it is vital to note that these plots are not exactly the same. For example, when $\kappa = 0.1$, the shortening factor has a minimum of approximately 0.9965 as seen in Figure 5.1 (b), while when $\kappa = 0.01$, the shortening factor has a higher minimum of approximately 0.9997 as seen in Figure 5.6 (b). Thus, we can observe that for stronger coupling of the electrical excitation to the calcium signaling component of the model the cell contracts more. This is fundamentally the expected behavior, since stronger coupling from the voltage to the calcium system should make the effect of contraction more pronounced.

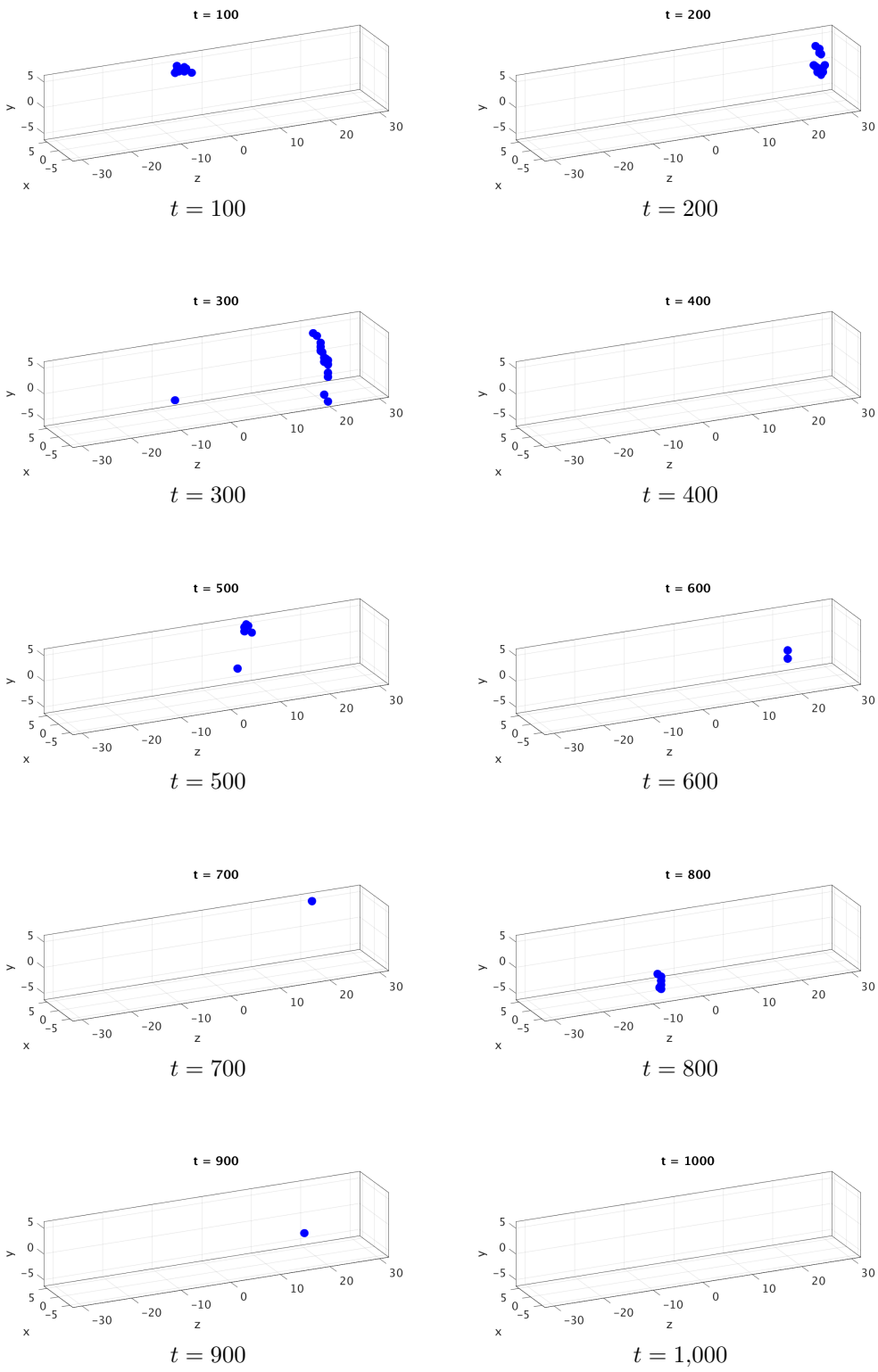

Figure 5.7: Open calcium release units throughout the cell for $\kappa = 0.01$.

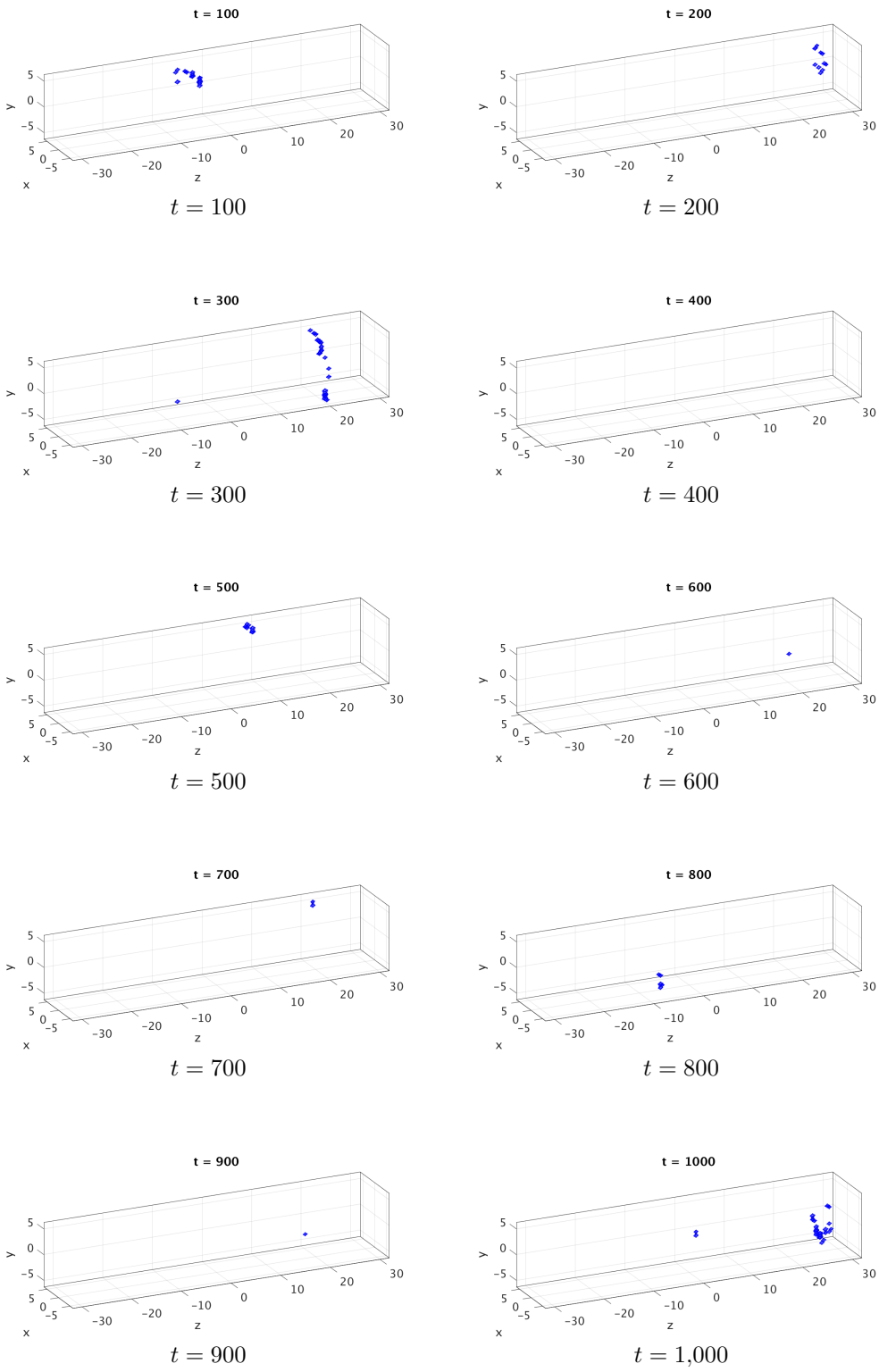

Figure 5.8: Concentration of $c(\mathbf{x}, t)$ throughout the cell for $\kappa = 0.01$, with a critical value of 65 μM.

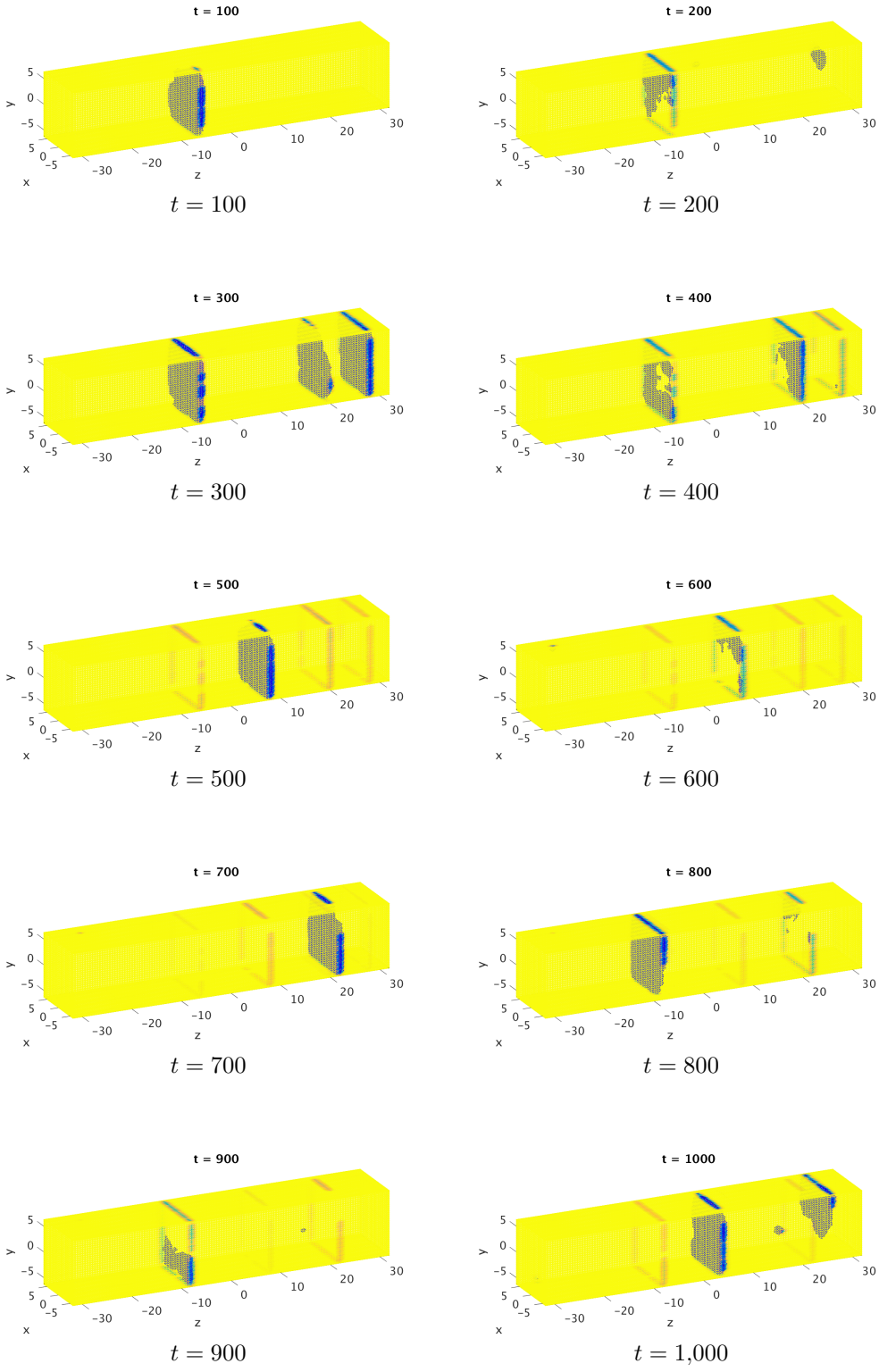

Figure 5.9: Concentration of ${b_3}^{(c)}(\mathbf{x}, t)$ throughout the cell for $\kappa = 0.01$, with a critical value of 120 μM.

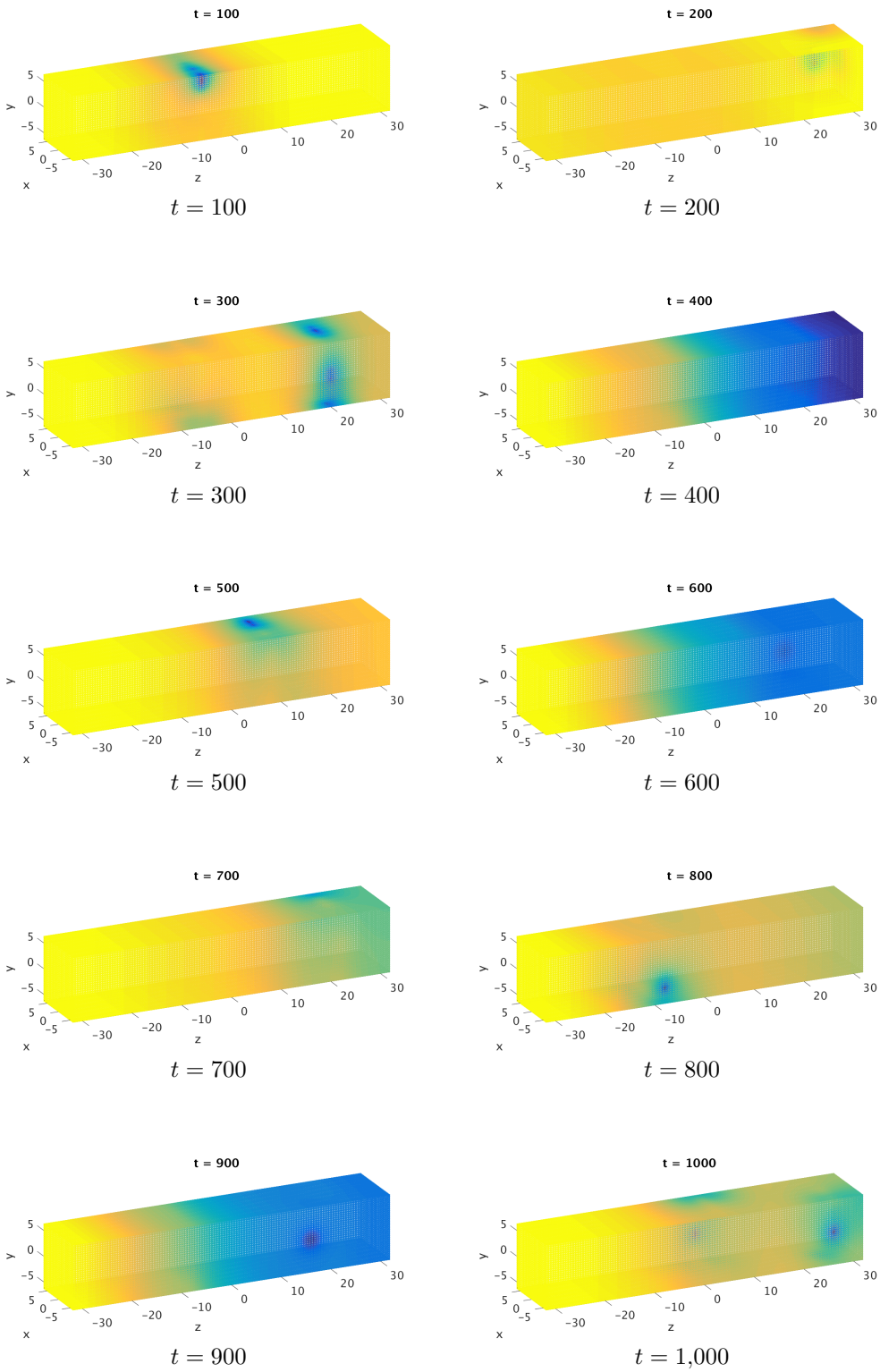

Figure 5.10: Concentration of $s(\mathbf{x}, t)$ throughout the cell for $\kappa = 0.01$, with a critical value of 5,000 μM.

6 Conclusions

We now have a working seven variable model which includes for the first time the mechanical component of the excitation-contraction coupling (ECC) cycle in a heart cell. In the simulations, this is accomplished by including the third cytosol buffer species, the inactive actin-myosin cross-bridges, and the links ③ and ④ in Figure 1.1. Through simulations, we analyzed specific cases of coupling strength κ from the electrical to the calcium system to get a better understanding of the behavior of the model. From the results we notice that while modifying the κ value does not affect voltage significantly, it impacts many of the other species in the model including the cell's contraction. This is clear as we see differences in the plots of the shortening factor for the different sets of model parameters. The plots show that the contraction behavior mirrors that of the voltage and shows a realistic representation of what is physiologically happening.

Because the plots of the shortening factor are not ideal to our understanding, future research done on this topic should include further parameter studies in order to get more reasonable behavior of the cell contraction. Once this is established, the model can be extended to include the eighth variable already proposed in [1].

Acknowledgments

These results were obtained as part of the REU Site: Interdisciplinary Program in High Performance Computing (`hpcreu.umbc.edu`) in the Department of Mathematics and Statistics at the University of Maryland, Baltimore County (UMBC) in Summer 2017. This program is funded by the National Science Foundation (NSF), the National Security Agency (NSA), and the Department of Defense (DOD), with additional support from UMBC, the Department of Mathematics and Statistics, the Center for Interdisciplinary Research and Consulting (CIRC), and the UMBC High Performance Computing Facility (HPCF). HPCF is supported by the U.S. National Science Foundation through the MRI program (grant nos. CNS–0821258 and CNS–1228778) and the SCREMS program (grant no. DMS–0821311), with additional substantial support from UMBC. Co-authors Nygel Foster, and Darius Leftwich were supported, in part, by the UMBC National Security Agency (NSA) Scholars Program through a contract with the NSA. Graduate assistant Carlos Barajas was supported by UMBC. All of us thank Dr. Brad Peercy for invaluable discussions on the background and goals of mathematical physiology.

References

[1] A. M. Alexander, E. K. DeNardo, E. Frazier III, M. McCauley, N. Rojina, Z. Coulibaly, B. E. Peercy, and L. T. Izu. Spontaneous calcium release in cardiac myocytes: Store overload and electrical dynamics. *Spora: A Journal of Biomathematics*, 1, 2015.

[2] K. Angeloff, C. Barajas, A. D. Middleton, U. Osia, J. S. Graf, M. K. Gobbert, and Z. Coulibaly. Examining the effect of introducing a link from electrical excitation to calcium dynamics in a cardiomyocyte. *Spora: A Journal of Biomathematics*, 2, 2016.

[3] T. Banyasz, B. Horvath, Z. Jian, L. T. Izu, and Y. Chen-Izu. Profile of L-type Ca 2+ current and Na+/Ca 2+ exchange current during cardiac action potential in ventricular myocytes. *Heart Rhythm*, 9(1):134–142, 2012.

[4] K. Deetz, N. Foster, D. Leftwich, C. Meyer, S. Patel, C. Barajas, M. K. Gobbert, and Z. Coulibaly. Developing the coupling of the mechanical to the electrical and calcium systems in a heart cell. Technical Report HPCF–2017–15, UMBC High Performance Computing Facility, University of Maryland, Baltimore County, 2017.

[5] X. Huang, M. K. Gobbert, B. E. Peercy, S. Kopecz, P. Birken, and A. Meister. Order investigation of scalable memory-efficient finite volume methods for parabolic advection-diffusion-reaction equations with point sources, In preparation (2017).

[6] L. T. Izu, J. R. H. Mauban, C. W. Balke, and W. G. Wier. Large currents generate cardiac Ca^{2+} sparks. *Biophys. J.*, 80:88–102, 2001.

[7] L. T. Izu, W. G. Wier, and C. W. Balke. Evolution of cardiac calcium waves from stochastic calcium sparks. *Biophys. J.*, 80:103–120, 2001.

[8] C. Morris and H. Lecar. Voltage oscillations in the barnacle giant muscle fiber. *Biophys. J.*, 35(1):193, 1981.

[9] B. Mozaffarian et al. Heart disease and stroke statistics — 2015 update: A report from the american heart association. *Circulation*, 131(4):e29, 2014.

[10] J. Schäfer, X. Huang, S. Kopecz, P. Birken, M. K. Gobbert, and A. Meister. A memory-efficient finite volume method for advection-diffusion-reaction systems with non-smooth sources. *Numer. Methods Partial Differential Equations*, 31(1):143–167, 2015.